



Tailored laser beam shapes for welding of copper using green laser radiation

Florian Kaufmann^{1,2} · Stephan Roth^{1,3} · Michael Schmidt^{1,3,4}

Received: 31 January 2024 / Accepted: 31 January 2024
© The Author(s) 2024

Abstract

The rapid development of laser beam sources and adapted welding technologies in recent years lead to an increased use of laser welding techniques in automated production nowadays. Especially its precision and local energy input are key features for joining applications in electric vehicle components, where joints have to meet both mechanical and electrical requirements as current-carrying connections. However, the copper materials used are difficult to weld due to their physical properties, making a stable process with fewest seam imperfections only feasible within a limited process window. Recently available beam sources emitting visible laser radiation have proven to overcome the low absorptivity at process start, but spattering is still a prone defect significantly affecting process efficiency and quality. Literature approaches for modifying the energy input point to laser beam shaping as a method for reducing process imperfections, which, however, has not been extensively researched in copper processing using green laser radiation.

Thus, this study investigates the influence of a shaped intensity profile for visible laser radiation created with a reflective diffractive optical element in laser beam welding with laser powers up to 3 kW. A characterization of the process dynamics is performed by use of high-speed imaging, and metallographic analysis is used to elaborate benefits of the applied beam shapes. With beam shaping, an enlarged heat conduction welding regime and an advantageous seam shape are found. Furthermore, a decrease in spatter formation during deep penetration welding is detected for the elliptical beam profile, which correlates with an oscillation movement of the capillary.

Keywords Laser beam welding · Beam shaping · Diffractive optical element · Copper · Green laser radiation · Process observation

1 Introduction

Contemporary ecological, economical, and social changes are leading to a transformation in the development, design, and production of future vehicles. Particularly encouraged by stricter homologation regulations and carbon pricing, the

stated goal of car manufacturers is to advance the development of environment-friendly vehicles and climate-neutral production throughout the supply chain [1]. The disruptive technological shift towards electric and hydrogen mobility requires an efficient and high-quality production of batteries, battery packs, power electronics, and electric drives [2]. An essential raw material in this sector is copper. Copper is seen as a green-energy transition player, partly because of the wiring needed for electric cars. Electric vehicles can use as much as 90 kgs of copper, which is three to four times more than in the case of a traditional combustion engine vehicle [3]. Higher demand and growing prices for the raw material are driving the research and expansion of suitable processing technologies, especially of joining processes capable of generating low resistance interconnections with high efficiency and automatability for large-scale production [4]. In this context, laser beam welding of copper is a key technology that reveals new opportunities by the use of visible

✉ Florian Kaufmann
f.kaufmann@blz.org

¹ Bayerisches Laserzentrum GmbH (Blz), Konrad-Zuse-Str. 2-6, 91052 Erlangen, Germany

² Friedrich-Alexander Universität Erlangen-Nürnberg, Schloßplatz 4, 91054 Erlangen, Germany

³ Erlangen Graduate School in Advanced Optical Technologies (SAOT), Paul-Gordan-Str. 6, 91052 Erlangen, Germany

⁴ Institute of Photonic Technologies (LPT), Friedrich-Alexander Universität Erlangen-Nürnberg, Konrad-Zuse-Str. 3/5, 91052 Erlangen, Germany

laser radiation. Due to the local, non-contact energy input, the flexibility in the design of the interconnection area, and the high automation capability, the technology offers great potential for joints of metallic materials [5].

In general, the physical properties of copper like the high thermal conductivity and low melt viscosity impede the welding process compared to steel. Altered optical properties aside from conventional infrared laser beam sources when using for example green laser radiation ($\lambda = 515 \text{ nm}$) show a changed energy coupling into the material [6]. A significant effect on process performance in terms of weld seam geometry is reported; however, the altered occurrence of seam imperfections (especially spatter formation) is aimed to be further reduced, and the deeper understanding of the necessary manipulation on the underlying physical phenomena to achieve a desired weld is of broad interest.

Approaches presented in the literature for modifying the energy input into the capillary, especially at its front wall, to reduce the formation of process imperfections during deep penetration welding point out the use of laser beam shaping as a method to influence process imperfections in a targeted manner [7].

Therefore, the goal of the presented work is to clearly identify the process windows for welding with different shaped laser beams to increase productivity and reduce defects. The influence of the beam shape on melt pool dynamics and vapor capillary behavior is investigated. Comparing *ex situ* analyses with high-speed observations of the interaction zone yields further insight and enhances process understanding when using shaped beam profiles in laser beam welding of copper with 515 nm laser radiation.

2 State of the art

2.1 Laser beam welding of copper

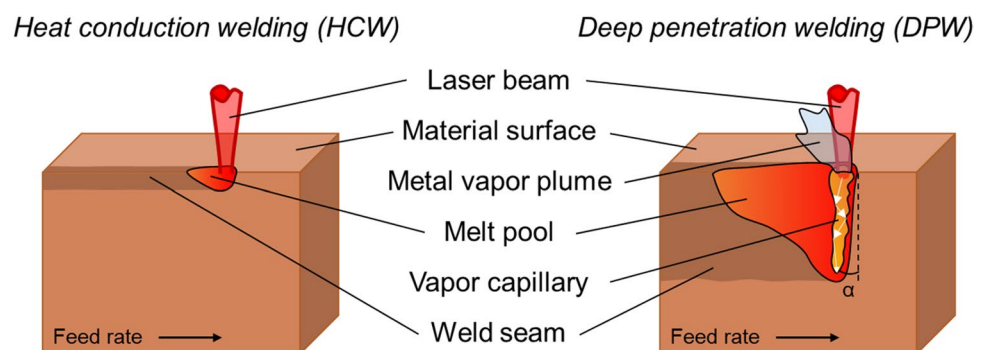
The process of laser beam welding can be subdivided into different regimes, heat conduction welding (HCW), and deep penetration welding (DPW). These two welding modes are shown in Fig. 1.

The regimes are run through in successive stages until the deep penetration threshold is exceeded in the case of DPW. Initially, the metal is heated by the absorption of the irradiated laser beam, depending on the used wavelength, material, surface conditions, and the characteristics of the laser beam. Once the melting point is exceeded, a melt pool starts to form in the interaction zone, resulting in the formation of a weld seam through the continuous movement of the beam—the heat conduction welding process (Fig. 1 left). The continuous temperature increase of the metal surface leads to a change in the degree of energy coupling [8]. As the energy transport into deeper layers is based on heat conduction, the achievable aspect ratio of the weld seam (penetration depth e to seam width w) does not exceed one, making HCW predominantly used in foil joining [9] and additive manufacturing [10].

The increasing recoil pressure of evaporation with further heating leads to a concave deformation and the formation of a depression in the melt pool, which enables further beam reflections. The opening vapor channel (also called keyhole) guides the laser beam by multiple reflections on its wall into the material, resulting in weld seams with high aspect ratio $\gg 1$ [11]. A metal vapor plume forms from the metal vapor emanating from the capillary, and the molten material is displaced by the acting pressure forces, causing melt pool flows and dynamics. Dependent on the processing parameters, the inclination angle α of the capillary front wall against feed direction influences the distribution of the absorbed energy in the interaction area [6]. As these characteristics lead to an efficient use of the deployed energy and facilitate processing of metal in the millimeter-range with a laser spot of a few hundred microns in diameter, DPW is frequently applied for laser welding of copper materials.

For copper, it is particularly challenging to generate a stable deep penetration welding process at moderate feed rates ($v \leq 6 \text{ m/min}$) using conventional near-infrared (NIR) lasers, which are well researched for material processing [12]. This circumstance is attributed to its physical properties: For wavelengths $\lambda \geq 1 \mu\text{m}$, the absorptivity of copper at room temperature is reported in the low single-digit range and increases erratically at the transition from solid to liquid

Fig. 1 Schematic sketches of heat conduction welding (left) and deep penetration welding mode (right)



state to approximately 14% at 1 μm [13]. In addition, the phase change is associated with an abrupt decrease of the thermal conductivity in the molten state, which is unfavorable for the welding process due to an accumulation of the heat in the interaction zone [14]. As a result, spatter formation is promoted, and increased melt ejection and poor seam appearance are reported [15].

Strategies to improve the energy coupling of copper comprise a modification of the workpiece surface, e.g., by roughening or laser structuring [16]. Other methods include the coating of the workpiece with less reflective materials such as nickel or tin, as well as obscuring the surface by oxidation at high temperatures [17]. For industrial applications, changing the processing wavelength to blue [18] or green radiation [19] is considered a target-oriented strategy to significantly enhance the efficiency and reproducibility of the copper welding process. For 515 nm laser radiation at room temperature, absorptivity values around $A=40\text{--}50\%$ are reported, and there is no change over temperature of the same order of magnitude as for NIR radiation. Due to the improved energy coupling at first laser-matter interaction, less energy is required to reach the melting and evaporation temperature of the copper material, thus extending the process window for deep penetration welding [20]. Nevertheless, spatter formation still remains a challenge for process stability and efficiency even using visible laser radiation [21]. In general, a stable welding process is characterized by consistent and satisfactory welding results, i.e., low fluctuations in the seam geometry regarding penetration depth and seam width, and a low incidence of defects, especially pores and spatter [22].

2.2 Weld seam imperfections caused by process dynamics

The most common weld seam imperfections in copper welding are pores, spatter, melt ejections with subsequent hole formation, and seam root collapse [23].

Pores and voids are characterized as spherical gas-containing inclusions, with a distinction being made between gas and process pores [24]. The former are usually associated with the precipitation of dissolved gases during solidification, thus having minor connection to the dynamics of the laser welding process. The latter are inclusions of inert gas or metal vapor [25]. The authors in [26] conclude that small pores (diameter < 16 μm) can be classified as uncritical for seam performance as long as there are no agglomerates in pore clouds. When welding copper using 515 nm wavelength, a higher porosity was observed in the investigations in [20] compared to NIR laser radiation; however, this welding process showed the most stable results with the least fluctuations.

Holes are mechanically and electrically critical defects, as they induce stress peaks in the weld seam and reduce the

effective interconnection area, thereby increasing the contact resistance of the joint. These imperfections are typically observed as a result of melt ejections or particularly large spatters, predominately detected at feed rates $v < 8$ m/min [27]. The emergence of large melt ejections is attributed to short time instabilities (dynamic variation of the absorbed energy in the vapor capillary) of the deep penetration welding process and the consecutive formation of a vapor bulge in the lower capillary area. Once this bulge against feed direction grows in size rapidly, increasing vapor pressure can exceed the surface tension of the melt pool so that parts of it or, in extreme cases, the complete surrounding melt pool are ejected. This bulging phenomenon arises as a result of a small capillary front wall inclination relative to the beam axis, since the irradiated laser power at the front wall is reflected preferably into the lower capillary area, inducing strong fluctuations there [28]. In addition, the capillary bulging in copper welding was found to show different intensities depending on the laser wavelength and is related to the surface quality of the final weld [6].

Small spatters only have a minor influence on the surface quality of the weld seam, but can contaminate surrounding components of an assembly, the clamping device, or optical components. These small metal droplets, which are entrained by escaping metal vapor from the capillary, possess comparable high velocities (up to tens of m/s; spatter release criterion [29]), making their contamination area large. Typical spatter dimensions are reported with 50–200 μm diameter, with a decreasing probability of occurrence observed with reduced laser power and increased feed rate, accompanied by a changed spatter release position [30]. In summary, a number of important findings have been reported on the formation mechanisms of process instabilities, but their effective reduction in copper welding using green laser radiation remains largely unexplored.

2.3 Beam shaping and influence on process stabilization

Approaches to stabilize the welding process with regard to seam imperfections comprise a modification of the ambient conditions [31], the melt pool [32], the vapor capillary [33], as well as influencing the energy input into the latter [7]. When looking at the reported successful methods for influencing weld seam imperfections, it becomes clear that for a reduction of these, an energy input at the capillary wall must be applied, which avoids locally increased evaporation at certain capillary areas. Beam shaping of the intensity profile offers the possibility of a variation of these input variables.

There are different methods of beam shaping. Considering the complexity of shaping and its practicality, especially the methods, aspheric lens group shaping, liquid crystal spatial light modulation shaping, microlens array shaping,

and diffractive optical element shaping (DOEs) are of broad applicability [34]. A wide range of focal intensity profiles can be achieved by using DOEs. By applying structures to optical elements with high diffraction efficiency (DOE), the intensity profile can be changed almost arbitrarily by the use of interference (based on the theory of diffractive optics) [35]. Industrial application of the DOE technique for beam shaping can be found in micromachining, e.g., for fast, simultaneous drilling of microholes [36].

Investigations on shaped laser beams by DOEs in metal welding [37] demonstrate that weld seams with an almost rectangular cross-section can be obtained by multi-spot keyhole welding of steels. The authors in [38] used a shaped laser beam by DOE in combination with beam oscillation for welding aluminum alloy, reporting a more stable melt pool due to the uniform energy distribution compared to conventional gaussian beam welding. Sundqvist et al. present studies focusing on the numerical and analytical optimization of laser spot welding with shaped laser beams [39]. Using a semi-analytical model, the author in [40] confirms that capillary geometries resulting from different beam shapes induce differing pressure gradients that affect the dynamic behavior of the welding process (detected oscillations). Especially the use of an elliptical beam as a transition from conventional round beams shows improvements in simulative and experimental studies, tailoring the interaction zone and solidification conditions [34].

Matthews et al. [41] studied the effect of elliptical beams on the melt pool state, finding that a regulation of the surface morphology and of the microstructure of components with specific structures becomes possible. Using the ellipse either as a longitudinal ellipse beam (long axis parallel to the feed rate) with a wider energy distribution area along the processing direction allows a longer heating and holding time in the interaction zone, or the rotation to a transversal ellipse result in larger undercooling and the generation of a finer grain structure. Based on his simulation model, Beck [42] describes that in order to increase the feed rate with limited maximum surface deformation, either the capillary (spot) diameter must be reduced or the melt pool width must be increased. This can be achieved by a linear beam shape that is moved in its narrower direction or by the combined use of several laser beams with beam foci positioned in line with each other in processing direction. Experiments by Glumann [43] with an elongated capillary shape, created by using two laser beams in line, showed that this setup can increase the maximum welding speed of ferrous materials by up to 50%. Abe et al. report the successful application of a focused elliptical beam of a direct diode laser to weld stainless steel foils with a thickness of 5 μm on thick substrates at a higher speed than a circular beam, observing a reduced heat affection to the substrate material [44]. Investigations based on a computational fluid dynamics approach to analyze the influence of beam shaping (a reference Gaussian profile and its elliptic elongation) in

welding on the melt thermal flow revealed that, apart from the intensity alteration and a change in the direction of the melt thermocapillary flow, the flow pattern also changes. For a longitudinal ellipse beam, melt front vortices that assist metal pre-heating are identified. It is concluded that the elongation of a beam profile has a non-linear effect on melt flow and in turn on the seam geometry as well as on the temperature gradients in the heat-affected zone [45]. Analyses for laser-based processing of high-strength aluminum alloys on the influence of different beam shapes based on single weld tracks in Ref [46] reveal that core/ring profiles have wider melt pools compared to a purely Gaussian beam. Furthermore, the weld seam width of the Gaussian beam profile is detected much more dependent on the laser power compared to the point/ring profiles studied. Investigations on copper using a similar beam shaping approach for 515 nm laser radiation show a process window extension, wherein the use of core/ring profiles allows for increased weld depths in Cu-ETP while preserving weld quality with a homogenous seam surface and shifting the process limitation of excessive spatter and melt ejection formation to lower feed rates [47]. This behavior is related to the observed widening of the capillary entrance and the inclination of its front wall, causing a more uniform evaporation in the capillary and stabilizing the welding process by reducing the melt dynamics.

In conclusion, the abovementioned papers show that non-standard beam shapes can have clear benefits for a wide range of welding applications; however, they are rarely used nowadays, especially in copper processing using emerging laser wavelengths like 515 nm. The major technical barrier for DOEs is assumed to be the complexity of predicting a beam shape irradiance profile to obtain the desired weld seam geometry, as the widely iterative trial-and-error approach is expensive and time-consuming [48]. Thus, the objective of this work is the experimental characterization of the process dynamics and weld seam imperfection formation in direct comparison of different laser beam shapes using process observation and metallographic analysis. Therefore, this study uses a welding setup capable of producing a top hat (flat-top) and an elliptical beam shaped by DOE for copper welding with 515 nm laser radiation to extend the fundamental process understanding.

3 Experimental setup and methods

3.1 Laser beam welding setup

For the experiments, a frequency-doubled disk laser TruDisk 3022 (Trumpf GmbH, Ditzingen, Germany) emitting 3 kW maximum cw-output power at $\lambda = 515$ nm wavelength was

used. The system properties and further properties of the optical setups are presented in Table 1.

The beam-delivery fiber coupled to the welding optics had a core diameter of $d_{LLK}=200\ \mu\text{m}$. Using a collimating length of $f_C=200\ \text{mm}$ and focusing lens with a focal length of $f_F=200\ \text{mm}$, a conventional top hat (TH) beam with a magnification ratio of 1:1 was obtained as the fiber end is imaged onto the focal plane. A spot diameter of $d_F=202.0\ \mu\text{m}$ in almost top hat intensity distribution was measured with a Primes Focus Monitor FM+ (Primes GmbH, Pfungstadt, Germany) for the optical setup. The measured intensity distribution in the focal plane is presented in Fig. 2 on the left.

A customized welding optics with a collimating lens of $f_C=100\ \text{mm}$ and a $f_F=60\ \text{mm}$ focusing lens was built for the elliptically shaped laser beam using a reflective DOE (supplier: Midel Photonics GmbH, Bonn, Germany). Its design is shown in Fig. 3.

As laser powers up to 3 kW are used and the process is accompanied by extensive heat build-up, the fiber plug is water cooled, while the lenses as well as the DOE and the 2" mirror are air cooled (air cooling not shown). For operational safety, failure barriers are installed behind the optical elements. For the DOE design, it is important to know the

diameter and intensity distribution of the laser beam at its position, which was measured using the knife-edge method and fitting with a super-Gaussian function. The beam collimation was checked by repeating this procedure at a distance of 200 mm and 300 mm from the lower edge of the collimating lens mount. For further calculations, a 1/e2 diameter of 20.7 mm was assumed, chosen to minimize the peak intensity of the beam on the DOE while avoiding a significant amount of laser power hitting the pivoting mirror mount if 1" DOEs are used. The angular alignment of the DOE and mirror (15° each) in the optical path was checked and iteratively optimized; the final result for the welding trials is shown in Fig. 2 on the right. The axes of the elliptical beam in the focal plane were measured to be 204.2 μm in the short axis and 366.1 μm in the long axis.

The final experimental setup is shown in Fig. 4. The welding optics were mounted successively on an industrial robot arm (KR30, Kuka AG, Augsburg, Germany) for the welding trials, allowing a precise adjustment of the spot orientation and working distance. For the investigations, sand-blasted copper samples (Cu-ETP, $t=3\ \text{mm}$, 50 mm × 30 mm) were fixed in the clamping device mounted on an axis stage ensuring a stationary process zone for high-speed process observation. Nitrogen was supplied through a lateral nozzle to cover the process zone and suppress plume interaction [49]. To protect the welding optics from spatter and metal fume, a compressed air-fed cross jet was installed. For the recording of the interaction zone throughout the entire weld seam length in side-view (x-z-plane), the sample was moved with feed rate v , while the optics and observation equipment were stationary. The process parameters investigated in the experimental campaign (full factorial experimental design) are listed in Table 2.

Table 1 Parameters and properties of the laser beam source and the optical setups used in this work

Parameter	Unit	Trumpf TruDisk 3022
Laser medium	-	Disc
Wavelength λ	nm	515
Laser power P_{max}	W	3000 cw
Fiber diameter d_{LLK}	μm	200
Focal diameter d_F	μm	202.0 (TH), 204.2 × 366.1 (EL)

Fig. 2 Measured intensity distribution for top hat (TH, left) and elliptical (EL, right) beam profiles at $P_L=1000\ \text{W}$ laser power

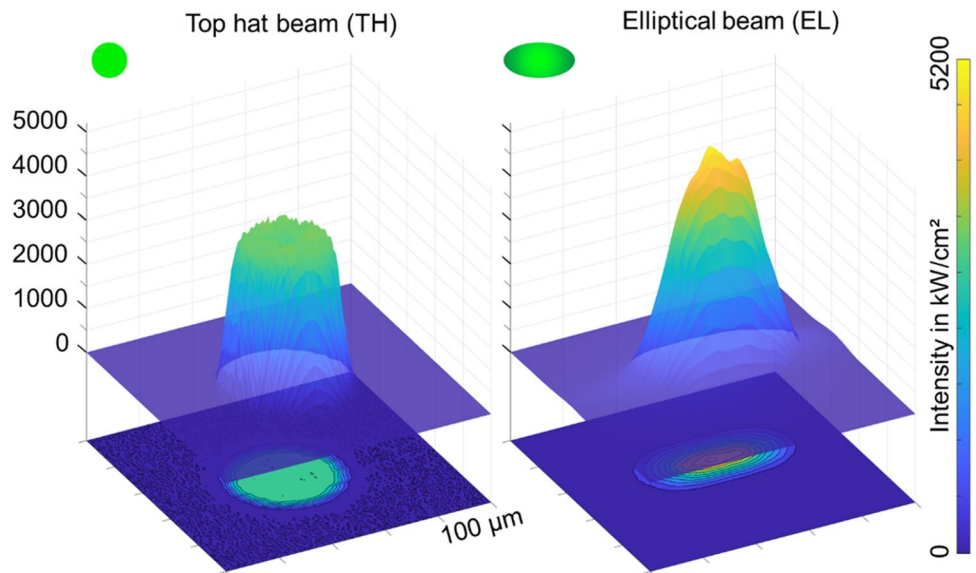


Fig. 3 Customized welding optics

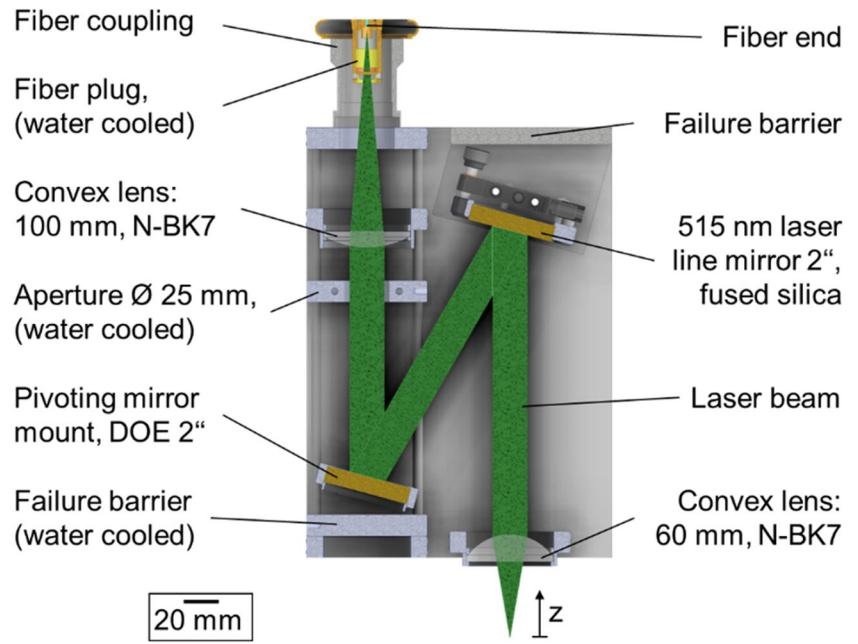


Fig. 4 Experimental setup used within this work. Green box: Insert: arrangement in the laser processing zone

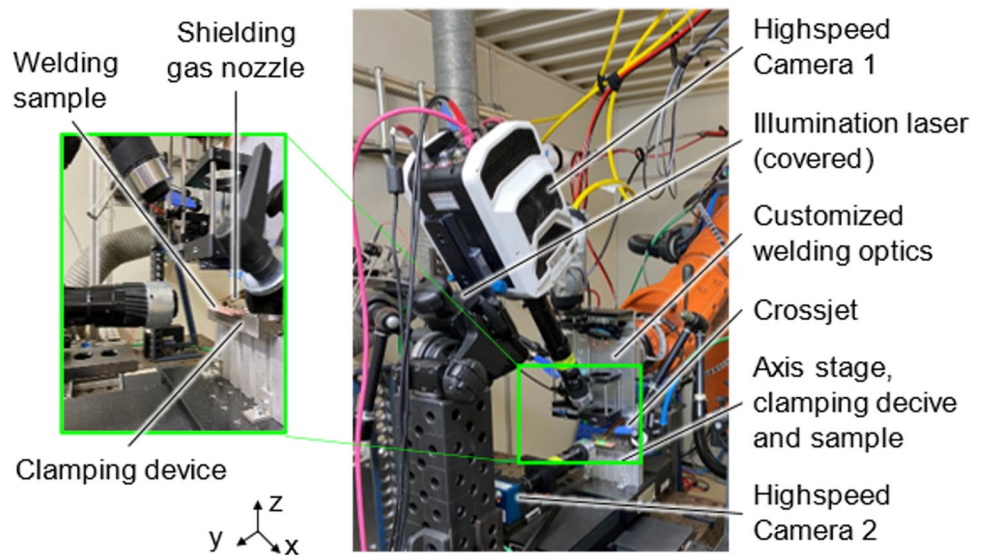


Table 2 Overview of the used process parameters for welding trials

Dimension	Unit	Choice of parameters
Material of sample	-	Cu-ETP
Beam profile	-	Top hat beam, elliptical beam
Feed rate v	m/min	2; 4; 6; 8; 10; 12; 14; 16; 18; 20
Laser power P_L	kW	0.5; 1; 1.5; 2; 2.5; 3
Focal position z_{Fok}	mm	0 (top surface)

Partial penetration welds of $l_{Weld}=45$ mm length were generated using the different laser beam profiles (see Fig. 2) and laser power ranging from $P_L=0.5-3$ kW, with feed rate

varied between $v=2-20$ m/min. The processing parameters were selected based on initial trials, including the transition point from HCW to DPW and avoiding a complete penetration of the sample. Mass loss owing to process instabilities (spatter, melt ejection, see Sect. 2.2) was quantified from weighing the specimens before and after the welding process using a precision balance (Sartorius Practum, Sartorius, Göttingen, Germany).

For process observation, two high-speed cameras (Phantom v1210, Vision Research, Wayne, United States and EoSens mini2, Mikrotron, Unterschleißheim, Germany) were used to monitor the capillary and melt pool dynamics. The videos from the former (Cam 1), mounted under an angle of

30° to the workpiece normal, were recorded at a resolution of 512×320 pixels with a frame rate of 50 kHz. The region of interest (ROI) in combination with a $12 \times$ zoom lens (Navitar, Rochester, NY, United States) is aligned for lateral observation of the interaction zone. Illumination of the welding area with a ns-pulsed diode laser (Cavitar Cavilux HF, $\lambda = 808$ nm, $P_{Avg} = 500$ W) and bandpass filtering (FBH810-10, Thorlabs GmbH, Newton, NJ, United States) ensured that the processing laser, plasma plume, and reflections from the interaction zone were blocked or reduced from the camera sensor. Additionally, while camera 1 monitors the welding process, camera 2 (Cam 2) is positioned perpendicular to the laser beam axis resulting in a sharp view on spatter formation and propagation. The videos of Cam 2 were recorded at a resolution of 592×428 pixels and a frame rate of 5 kHz. Since the intrinsic glow of the spatter was of interest, a longpass filter with a cut-on wavelength of 650 nm (FEL0650) was mounted in combination with blocking of the illumination wavelength.

3.2 Data evaluation: metallurgical preparation and image processing

After welding, surface and cross-sectional analyses were performed in a multi-step procedure. Before the samples were cut into 5 sections, the weld seams were analyzed in top view using microscopic images and a 3D profilometer (VR6000, Keyence Corp., Osaka, Japan). The samples were ground with up to 4000 grit and subsequently polished using a final grain size of 0.25 μm . To determine internal defects and grain morphology, etched (etchant: Fe(III)-Cl, etching time $t = 5$ s) metallographically prepared cross-sections were investigated. As an imaging resolution of 0.876 $\mu\text{m}/\text{pixel}$ was used, a measurement accuracy of at least 17.5 μm can be assumed for the minimum internal defect size. The defect evaluation was performed in a semi-automatic process based on image processing, described in more detail in [50]. For the characterization of the weld seam dimensions, electrolytically polished specimens were analyzed.

The high speed recordings of Cam 1 and Cam 2 were evaluated in regard to incoupling, capillary instabilities,

and spatter ejection. The capillary geometry was evaluated using the temporal average of the pixel values from Cam 1, taking into account all relevant images of the stationary welding process. A streak imaging approach was developed to investigate the dynamic behavior, whose workflow is presented in Fig. 5. For the analysis of lateral dynamics in width direction (capillary and melt pool width, spatter formation), the capillary length was initially measured from the temporal average image (see images 2 and 3 of Fig. 5) by analyzing the intensity profile. The maximum value from line-by-line evaluation was set as the capillary length l_{Cap} . The pixel column value of $l_{Cap} / 2$ was then used to generate the streak image by lining up the pixel columns at that position for each timestep of the video to create a new image representing temporal changes in the interaction zone (time on the horizontal axis). The rotation of this approach by 90 degrees creates streak images of the interaction zone orthogonal to the feed direction, allowing the temporal changes of l_{Cap} and the melt pool length to be studied.

Figure 6a shows the interaction zone during deep penetration welding ($t = 3$ mm, $\lambda = 515$ nm, TH, $d_F = 200$ μm , $P_L = 1500$ W, $v = 8$ m/min) in front view captured from Cam 2. Analyzing the extract from the irradiated area, the characteristic element metal vapor plume and spatter become visible. By the calculation of a maximum intensity projection, indicating the maximum intensity value for each pixel within a selected image amount representing a weld length of 5 mm, the spatter formation and plume behavior during copper welding were simultaneously accessible for the parameter sets (Fig. 6b).

In this work, the influence of laser beam shape on weld seam dimensions, vapor capillary behavior, and process stability in copper welding using green laser radiation was investigated in a broad parameter range. The results presented in the following create a database for welding process optimization in terms of beam profile, laser power and feed rate based on the target criteria penetration depth and minimum number of weld seam imperfections.

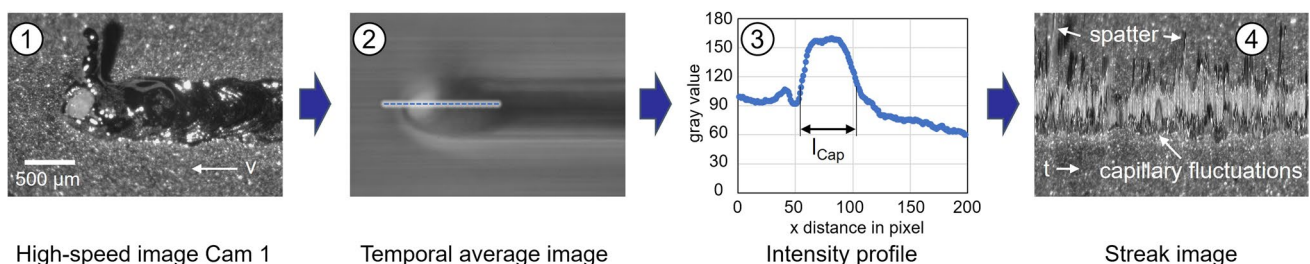


Fig. 5 Schematic illustration of the workflow for the calculation of a streak image of the vapor capillary width calculated for the pixel columns at the half capillary length ($l_{Cap}/2$) from high speed images of Cam 1

Fig. 6 **a** High-speed image of Cam 2 with schematic representation of the laser beam and **b** maximum intensity projection for laser beam welding of Cu-ETP $\lambda = 515$ nm, TH, $d_F = 200$ μm , $P_L = 1500$ W, and $v = 8$ m/min

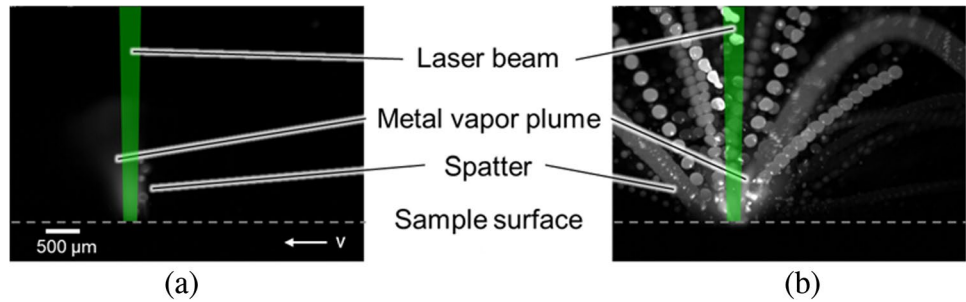


Table 3 Averaged measured laser powers ($t_{\text{Measure}} = 30$ s) for both welding optics used in this work

Set laser power	Measured laser power TH beam (reference welding optics)	Measured laser power EL beam (customized welding optics)
1000 W	1025.4 W	1018.5 W
3000 W	3084.7 W	3080.0 W

4 Results and discussion

4.1 Analyses of the welding optics and DOE’s performance

For the evaluation of the laser induced damage threshold of the DOE, the laser power on its surface was successively increased in steps of 100 W for a top hat beam of 150 μm diameter, since only a damage threshold for a pulsed laser process of 0.5 J/cm² for $t_p = 1$ ps at $\lambda = 515$ nm is known from the substrate supplier. The limit is determined to be 0.6 kW, corresponding to a peak intensity of 3.4 MW/cm², which indicates that the layout of the customized welding optics is well below this threshold. Moreover, the beam profiles of the customized welding optics with DOE and the reference optics with top hat beam were experimentally analyzed at different laser powers to investigate whether

changes could be observed. As no significant changes were found, the reflection efficiency was evaluated at a laser power of $P_L = 1$ kW and 3 kW to calibrate the laser power for the welding trials. The results are presented in Table 3.

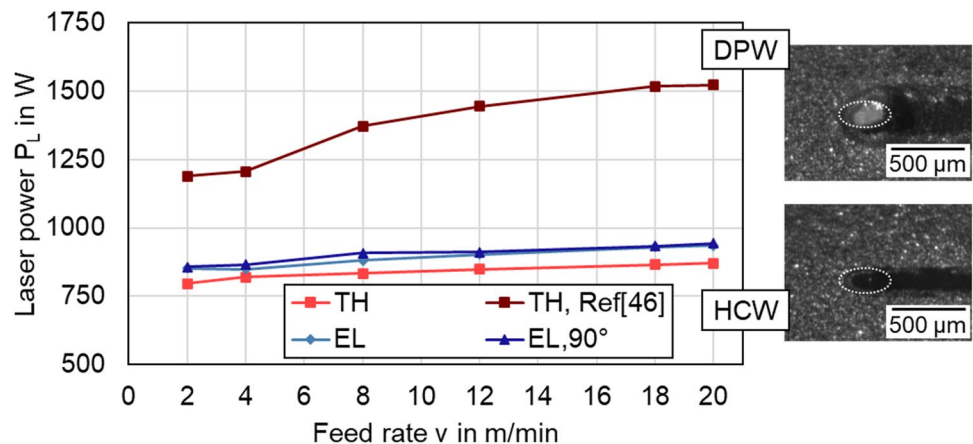
No significant losses are noted for the elliptical beam in the customized welding optics compared to the reference welding optics (BEO D70) without the additional optical elements. The reflection efficiency of the designed setup is therefore > 99% and is in good accordance with the specified data of the DOE of > 99% and the mirror of > 99.8%.

4.2 Process window for deep penetration welding

The deep penetration threshold (DPT), namely, the transition from HCW to DPW as a function of the feed rate v for the different beam profiles, which is derived from the analysis of the point of vapor capillary formation from high-speed videos with linearly increased laser power, is shown in Fig. 7. In the following, the configuration ellipse with the major axis coincident with the feed direction will be referred to as EL; the orientation rotated by 90 degrees will be referred to as “rotated ellipse” or “EL,90°.” In addition, the results of investigations using a top hat intensity distribution with $d_F = 340$ μm from [50] are included.

As in the transition zone, the energy balance is fulfilled for both HCW and DPW, but a melt pool depression with

Fig. 7 Deep penetration threshold for copper versus feed rate for varied beam profiles and exemplary high-speed images of process regimes DPW (top) and HCW (bottom) for beam profile EL, $\lambda = 515$ nm, and $v = 8$ m/min



evaporation characteristics is typically observed; this mode is assigned to DPW. It is a mixed mode regime between HCW and DPW that occurs when the power density is high enough to heat the material just above the vaporization threshold; however, the forming capillary does not extend to the melt pool front. A DPW process is present above the graphs in Fig. 7, while HCW takes place below (also see inserts on the right).

The standard deviation is not depicted for clarity but is found to be less than 5% for all datapoints and decreases with increasing feed rate for all beam profiles. The comparison with measured aspect ratios of the weld seams and changing surface characteristics (increased surface roughness and seam width at the onset of DPW) shows good agreement with the in situ analysis. This finding becomes exemplary evident from Fig. 8, where the rougher weld seam, a darker shade, and a jump in the joint width indicate the changed mode during the welding process.

For all investigated beam profiles within this work, a comparable dependence on the feed rate is observed, resulting in a 10% higher laser power for initiating a capillary when the feed rate is increased by a factor of 10. In comparison, a ratio of 25% and thus a stronger dependence on the feed rate for the increased TH spot diameter are observed in Ref. [50], indicating a higher heat conduction loss due to the larger irradiated area. This finding also applies to the comparison of TH and EL, as an earlier onset of DPW is found for the TH beam profile, yet not to the extent discussed above. The behavior can be attributed to the higher power density in the TH beam using the same selected laser power, thereby requiring less energy to reach target temperature T_{vap} (copper), which is in good agreement with Ref. [51] and experimental investigations in [47].

With regard to the orientation of the ellipse, no significant difference of the DPT between EL and EL,90° can be detected, generally providing a larger process window for heat conduction welding when using this beam profile. From the weld seam cross sections in Fig. 9, it can be clearly seen that especially the rotated ellipse achieves a wider remelted area compared to the other two beam profiles investigated, reflecting an advantage of the orientable beam shape. Thus, the joint can be tailored in weld seam appearance in HCW mode depending on the targeted application. This welding mode offers the advantage of a stable, almost spatter-free process for high-reflectivity metals like copper, which is predominantly feasible with visible laser radiation and almost nonexistent for NIR laser radiation [52].

4.3 Weld seam dimensions

However, due to the increased efficiency through multiple capillary internal reflections of the laser beam, deep penetration welding is widely used, which will be discussed in detail in the following sections. Since a widening of the interaction zone in width direction is of subordinate interest for industrial applications (exception: gap bridging, whereby this scenario is not taken into account in this work), predominantly TH and EL are investigated, as the heat distribution in lateral direction may cause increased distortion and enlargement of the heat-affected zone. The results of the cross-sectional analysis for the weld seam width w and the penetration depth e for both beam profiles are presented in Fig. 10 and Fig. 11.

For low feed rates $v \leq 6$ m/min, no significant difference in weld seam width is visible. An increase of the feed rate beyond this threshold causes a longer preservation of wider joints for the EL beam profile, indicating that the



Fig. 8 Top view of weld seam with increased laser power for constant feed rate: transition from HCW to DPW; beam profile EL,90°, $\lambda = 515$ nm, $P =$ varied, and $v = 8$ m/min



Fig. 9 Weld seam cross sections for varied beam profiles TH (left), EL (middle), and EL,90° (right) and indicated remelted area; $\lambda = 515$ nm, $P = 0.5$ kW, $v = 4$ m/min, feed direction indicated by white arrow

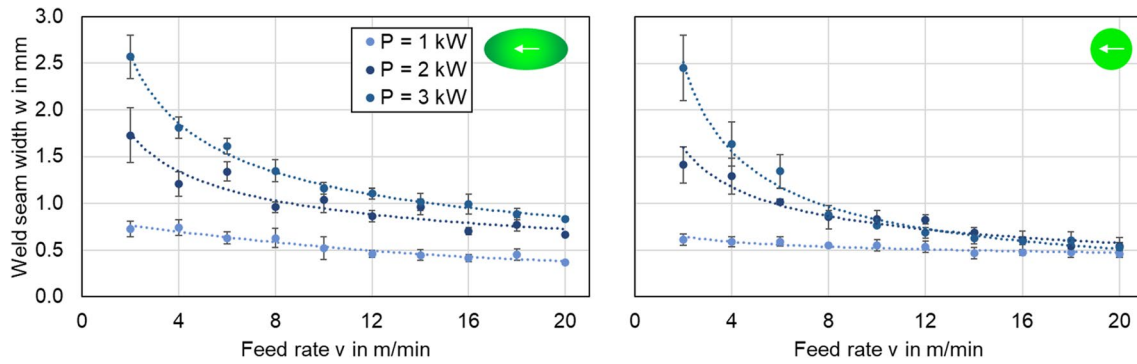


Fig. 10 Weld seam width w for different beam profiles EL (left) and TH (right) for a laser power of $P_L = 1\text{--}3$ kW and feed rate of $v = 2\text{--}20$ m/min; $\lambda = 515$ nm, Cu-ETP

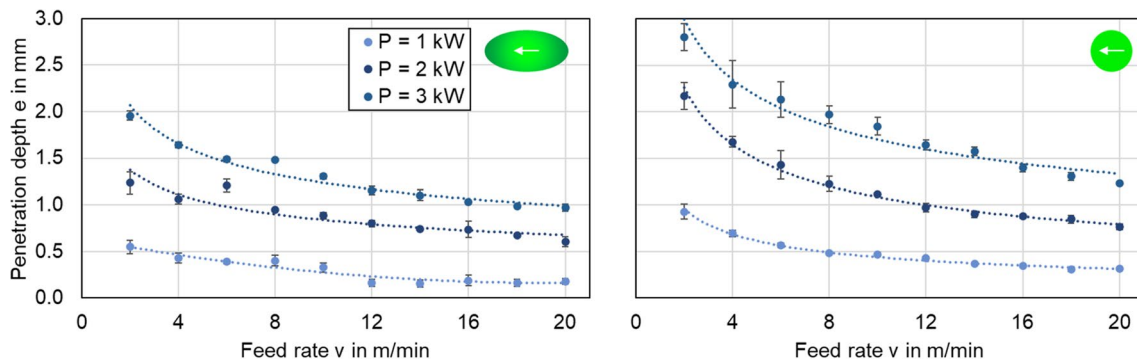


Fig. 11 Penetration depth e for different beam profiles EL (left) and TH (right) for a laser power of $P_L = 1\text{--}3$ kW and feed rate of $v = 2\text{--}20$ m/min; $\lambda = 515$ nm, Cu-ETP

temporally elongated irradiation leads to a wider distribution of the energy in lateral direction. As the laser power is increased, the weld seam width becomes wider, especially at low feed rates for both beam profiles, which is attributed to an increased heat accumulation in the irradiated zone.

The characterization of the penetration depth reveals different negative slopes with increased feed rate for varied beam profiles. The rate of decrease of e is found to be of higher value (larger negative exponent for the applied potency fit) in TH beam welding, while EL shows a lower dependency on the feed rate. The capillary depth decreases with increasing feed rate and reflection losses increase, while thermal conductivity losses decrease [42]. This phenomenon also leads to a reduction in weld seam width, which shows a decreasing trend for all settings investigated. Thus, deeper penetration can be achieved using the TH beam when applying the same laser power and feed rate. When a low dependence on the feed rate is required, the elliptical beam provides more stable results.

The standard deviation is found to be below 15% in all investigated processing parameter sets, decreasing significantly with increased feed rate for all beam profiles to values $\leq 5\%$. For the TH beam, increased geometric fluctuation

characteristics are observable at low feed rates in both the width and depth directions, which can be attributed to the increased dynamics due to the increased power density and thus evaporation. These results are in good accordance with investigations presented in [47] where the width of the seam is also found to be mainly affected by the ring part during welding with superimposed intensity distributions. When welding with constant total power while changing the distribution from core to ring welding, the decrease in core power reduces the penetration depth, while the seam width is affected to a minor extent except for pure core welding. The observed behavior of an increased feed rate dependency of the seam width for TH is also reinforced by the experimental investigations reported in [46].

When comparing equal penetration depth for TH and EL, the additional power for the latter beam profile decreases as the feed rate is equally increased. For example, a power difference of $\Delta P = 1$ kW is observed for the feed rate setting $v = 4$ m/min generating a penetration depth of $e \approx 1.6$ mm. This additional power decreases to $\Delta P = 0.5$ kW for $v = 8$ m/min (penetration depth $e \approx 1.5$ mm) and $v = 18$ m/min ($e \approx 0.85$ mm). The superimposed seam contours for different beam profiles are shown in Fig. 12.

Fig. 12 Superimposed seam contours for varied beam profiles (orange contour, EL; white contour, TH) and equal penetration depth; $\lambda=515$ nm, $P=2.5$ kW (EL)/2 kW (TH), $v=8$ m/min (left); $P=2.5$ kW (EL)/2 kW (TH), $v=18$ m/min (right)



At slower feed rates, the effect of heat dissipation from the interaction zone is more pronounced, causing a greater power difference due to the larger beam area of EL compared to TH at equal penetration depth. From the seam contour overlay, the wider joint area created by the elliptical beam can be identified, especially close to the sample upper surfaces. This behavior becomes less pronounced when the feed rate is increased. So a more V-shaped seam geometry is achieved using the elliptical beam profile, while steeper, straighter seam edges are observed for the TH beam.

Looking at the aspect ratio of the welds, calculated with the weld width at half penetration depth, as presented in Fig. 13, indicates largely constant values for EL as a function of the feed rate and a slightly decreasing tendency for TH as the feed rate is increased. The decrease for $P_L=1$ kW for $v > 10$ m/min is attributed to an incompletely developed deep penetration welding process that can be assigned to the transition mode, as observed from the corresponding high-speed images. It is noticeable that with EL, smaller aspect ratios are

obtained, which, however, can be kept constant versus increased feed rate compared to the TH beam profile. Increasing the laser power results in a vertical upward shift of the data points, which tend to be smaller for the EL beam, indicating higher energy coupling for the TH beam due to more constricted energy input and the high thermal conductivity of copper [53].

In Fig. 14, the aspect ratio is plotted for the weld seam width measurements at the top surface and at half the penetration depth. For reasons of visual clarity, the standard deviation is not shown in these diagrams.

As already discussed in the context of the weld seam geometry, the wide scattering of the results due to the high dynamics of copper welding becomes apparent when considering the aspect ratio at the sample surface. Overall, a broader distribution of the TH values with larger aspect ratios can be identified compared to the EL data points. Analyzing the results at half penetration depth, a pattern of values along a bisecting line can be observed. The smallest aspect ratios with values $<< 1$ are attributed to the HCW

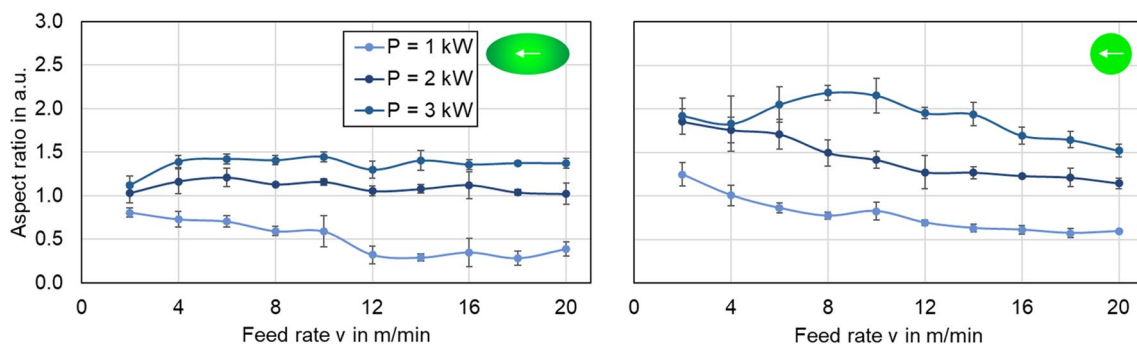


Fig. 13 Aspect ratio calculated with weld seam with at half penetration depth for different beam profiles EL (left) and TH (right) for a laser power of $P_L=1-3$ kW and feed rate of $v=2-20$ m/min; $\lambda=515$ nm, Cu-ETP

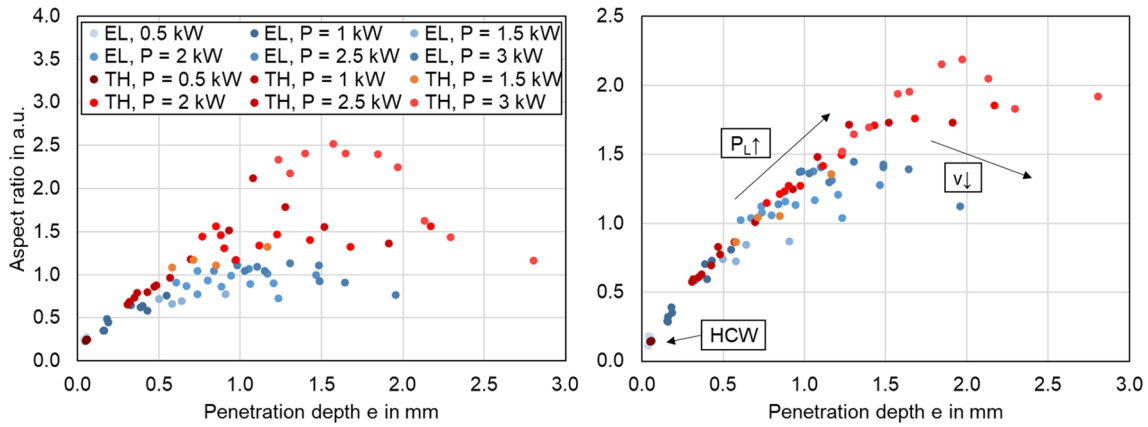


Fig. 14 Aspect ratio calculated with weld seam width at sample top surface (left) and at half penetration depth (right) versus penetration depth e for different beam profiles; $P_L = 0.5\text{--}3\text{ kW}$, $v = 2\text{--}20\text{ m/min}$

Table 4 Physical properties of copper and experimental conditions [52, 55]

Parameter	Unit	Copper
Density ρ	kg/m ³	8935
Melting temperature T_m	°C	1084
Ambient temperature T_0	°C	20
Thermal conductivity λ_{th} (T = 20 °C)	W/m*K	394
Specific heat capacity c (T = 20 °C)	J/kg*K	456
Latent heat of melting h_M	J/g	188

regime. Increasing the laser power results in deeper penetration and therefore higher aspect ratios (trend arrow “ $P_L \uparrow$ ”), while a reduction in feed rate causes the data points to advect to the right (increased penetration depth).

For further comparison of the beam shaping capabilities in copper welding, the melting efficiency (ME) is calculated according to Eq. (1). Based on Ref. [54], the latter indicates the proportion of energy consumed by the solid–liquid phase change in relation to the energy input and is computed as follows:

$$ME = [c \cdot (T_M - T_0) + h_M] \cdot \rho \cdot A \cdot v / P_L, \quad (1)$$

where ME is the melting efficiency, c is the specific heat capacity, T_M is the melting point temperature, T_0 is the room temperature, h_M is the latent heat of melting, ρ is the density, and A is the cross-section area. The parameter values for copper are listed in Table 4.

The results plotted versus penetration depth for varied laser power and feed rate (DPW mode) are shown in Fig. 15.

At low feed rates, a larger heat-affected zone is created and the thermal efficiency decreases (large melt pool volume which loses more energy). In accordance with these findings, the ME is observed to be decreased when small

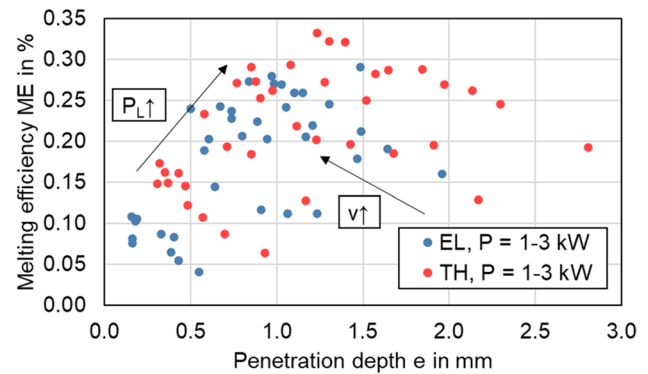


Fig. 15 Melting efficiency calculated according to Eq. (1) versus penetration depth e for different beam profiles; $P_L = 1\text{--}3\text{ kW}$, $v = 2\text{--}20\text{ m/min}$

feed rates are applied at a constant laser power for both beam profiles. Besides, the melting efficiency increases with the increase of the welding speed, which is also in good agreement with experimental studies on copper in [52]. Therefore, a 36% increased ME is found for the elliptical beam at a laser power of $P_L = 3\text{ kW}$, while a 72% increased value is detected for the TH beam when the feed rate is increased from $v = 2\text{ m/min}$ to $v = 20\text{ m/min}$. However, the lower feed rate dependence of EL welds observed earlier in this section is also reflected in a shallower increase in the ME data points with decreasing penetration depth. For equal processing parameters, a lower melting efficiency is observed for EL compared to TH. This behavior is attributed to the increased aspect ratio of the capillary (see Fig. 12) for the TH welding process, as the capillary internal reflections are thereby increased [42]. Nevertheless, the vapor capillary dynamics and weld seam imperfections have not been taken into account so far.

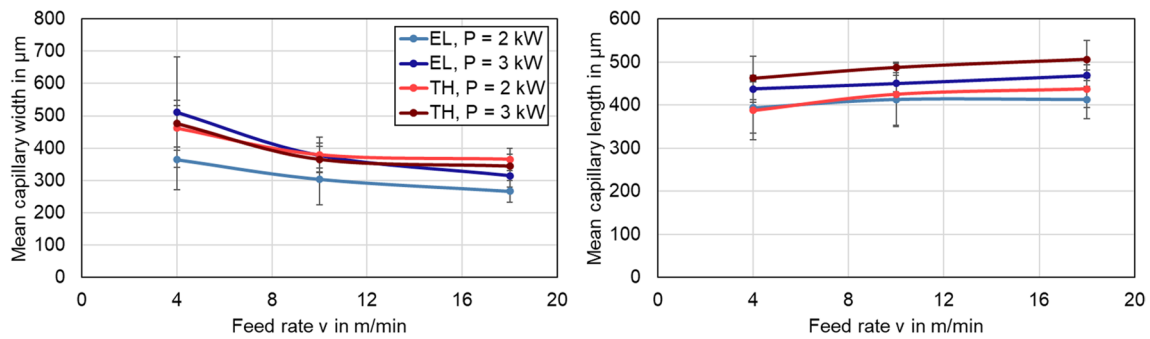


Fig. 16 Measured mean width (left) and length (right) of the capillary opening from high-speed observation versus feed rate v for different beam profiles TH and EL

4.4 Vapor capillary monitoring

The mean capillary length and width for both beam profiles obtained from streak image analysis for the EL and TH beam profiles are presented in Fig. 16.

For the capillary opening in the lateral direction (width), decreasing widths are observed when the feed rate is increased. This trend is found to be more pronounced for elliptical beam profiles, leading to a reduction of the mean capillary width by $\sim 100 \mu\text{m}$ when the feed rate is increased by 14 m/min, starting at $v = 4$ m/min and a laser power of $P_L = 2$ kW. This behavior is attributed to the elongated irradiance in the case of the EL beam profile, increasing the applied energy at any point in the laser matter interaction zone. The use of a higher laser power promotes this trend for the elliptical beam profile, whereas no significant difference is noted for the TH beam.

Considering the capillary opening in the welding direction, a feed rate dependent lengthening is observed for all laser powers investigated. The reason for this change originates from the inclination of the capillary front wall with increasing feed rate, inducing momentum of the evaporating material onto the capillary back wall [6] in

combination with a changing flow dominance from a surface tension gradient driven flow to a flow around the capillary. Additionally, the use of a higher laser power leads to an increase in the capillary opening area, calculated from the measured feature values assuming an elliptical opening, which can be explained by the increased absorbed energy in the irradiated area. These results agree well with the investigations reported in [21].

Overall, higher standard deviation values are found at lower feed rates, which can be attributed to increased process dynamics due to heat accumulation. In these statistical values, especially the data points for EL in the width direction are noteworthy. A further analysis of the temporal width variations based on the streak images reveals a periodic oscillatory movement of the capillary in the irradiated zone, illustrated in Fig. 17 for a laser power of $P_L = 3$ kW at a feed rate of $v = 4$ m/min. The subsequent evaluation by means of mathematical description as a harmonic oscillation is shown in Fig. 18. In this context, the oscillation amplitude is specified as the difference between the maximum capillary width and the baseline for the streak images in feed rate direction (compare Sect. 3.2).

Fig. 17 Streak images of the interaction zone in width (y) and feed (x) direction for laser beam welding of copper using an elliptical beam profile, $\lambda = 515$ nm, $P_L = 3$ kW, and $v = 4$ m/min

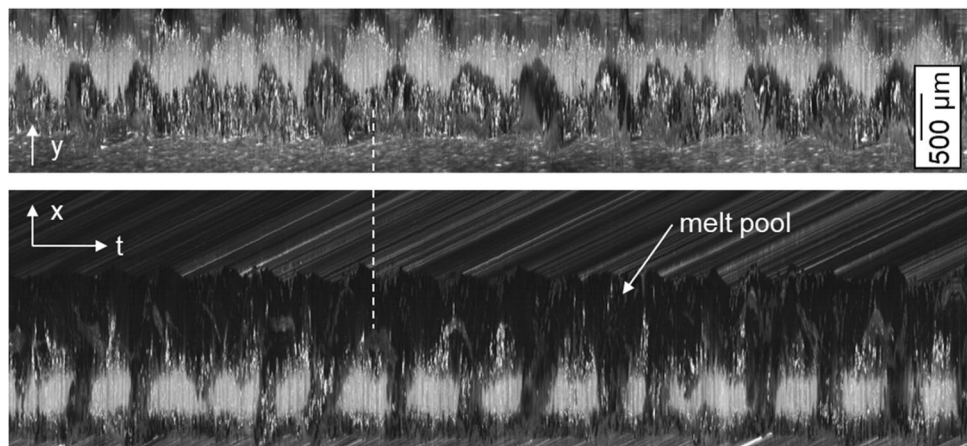
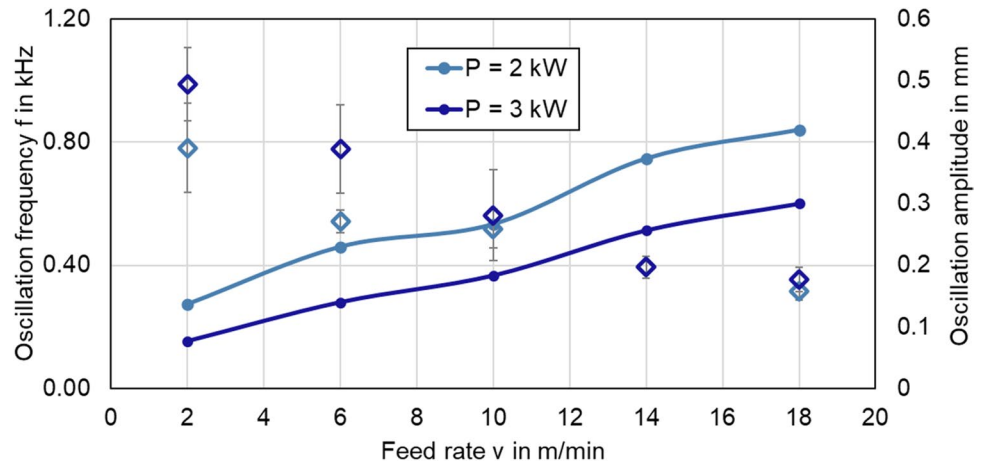


Fig. 18 Oscillation frequency and oscillation amplitude evaluated from streak images of the interaction zone versus feed rate for varied laser power during laser beam welding of copper using an elliptical beam profile



It becomes apparent that the streak images show oscillatory movements in and across the feed direction, with the features being linked in both directions. The points of maximum width coincide with the points of maximum capillary length, as indicated by the dashed line in Fig. 17. This movement is transferred to the melt pool, which also shows a periodically fluctuating tail. When analyzing the TH datasets, behavior of this kind is not observed. The reflection of the oscillation data for the process parameter window indicates an increase in frequency with increasing feed rate as well as increased laser power. At the same time, the amplitude decreases for the detected higher frequencies.

The behavior observed is assumed to be attributable to the fluctuating energy absorption in the interaction zone as a complex interaction of irradiated energy, attenuation, and disturbance effects like the metal vapor plume [49] and the observed time-varying capillary geometry (opening as well as geometric fluctuations in depth direction [6]). Another factor is the coupling with the surrounding liquid metal in the melt pool, which is more extensive in the case of the elliptical beam due to the lower-energy density boundary region in comparison to the TH beam profile. The comparison of these findings with results of other experimental process dynamic analyses summarized in [7] reveals similar time scales for the oscillatory movements.

Thus, the modified beam profile using an ellipse in copper welding using green laser radiation results in regular oscillating feature movements in the interaction zone. The authors in [56] state that a capillary without depth variations, without pore formation, and with a constantly high efficiency is required for a stable welding process. However, it has already been shown that a modulation of the laser power, as investigated in [27], can also stabilize the laser welding process of copper. The observed positive effects of the elliptical beam shape on the formation of seam imperfections are therefore discussed below.

4.5 Seam imperfection formation

Spatter ejection from the laser matter interaction zone and the melt pool was evaluated by means of maximum intensity projections and visual inspection of the recorded high-speed videos from Cam 1 and Cam 2. The resulting spatter count per 5 mm weld seam length as a function of feed rate for laser powers of $P_L = 2$ kW and 3 kW is presented in Fig. 19.

In general, the EL beam profile features a reduced spatter amount compared to TH over the entire processing parameter range investigated. An increase in the feed rate leads so a significant decline in spatter count, resulting in a 93% feature reduction for EL, $P_L = 3$ kW between $v = 2$ m/min and $v = 20$ m/min at the maximum. Increasing the laser power in connection with increased aspect ratio of the weld seam (see Sect. 4.3) is observed causing an upward shift of the data points for TH, while no dependency is found for the elliptical beam profile. The standard deviation (data not shown here for clarity reasons) is observed to be less than 5%, decreasing with increasing feed rate for both beam profiles. Comparing the evaluation with results for a wider TH beam diameter (340 μm in [50]), lower values are determined for the latter.

A significant difference in the size of the ejected particles is identified between EL and TH. On average, 41% smaller spatter are measured for the elliptical beam compared to the TH beam. The maximum intensity projection analysis shows the differences during the welding process in a demonstrative manner. Figure 20 shows exemplary results for comparable penetration depth of $e \approx 1.1$ mm for both beam profiles applying a feed rate of $v = 4$ m/min.

The significantly larger number of spatters can be recognized from visual inspection of Fig. 20. For the elliptical beam profile, however, the metal vapor plume is detected to be more prominent in laser irradiation direction. This behavior is attributed to a more uniform evaporation in the case of EL even at low welding speeds in comparison to

an increasingly fluctuating plume when using the TH beam profile.

The investigation of seam imperfection formation furthermore reveals a feed rate dependency, which is reflected in a predominant detachment of smaller spatters at higher feed rates. A maximum intensity projection and an example high speed image from the interaction zone for laser beam welding of Cu-ETP using a TH beam profile at a laser power of $P_L = 2500$ W and a feed rate of $v = 18$ m/min are shown in Fig. 21. Concerning the detachment point of the spatter at low feed rate, a larger fraction arises in the direction of the solid copper interface at the capillary front wall (see broad distribution in Fig. 14 for EL and TH). When the feed rate is

increased, the mechanism is observed to be shifted towards the back wall of the capillary and the melt pool, associated with a smaller angular range for material ejection almost exclusively against the feed direction. This phenomenon was observed independent of the beam profile used.

The observations made in this work can be corroborated based on findings of other researchers reporting that small detached particles move significantly faster than larger melt droplets (increased spatial difference in maximum intensity projection between Fig. 20 and Fig. 21) [30] and observing spatter occurrence mainly in the DPW mode [52]. Weberpals stated that due to the correlation between the inclination of the capillary front wall and the dynamic pressure

Fig. 19 Spatter count per 5 mm weld seam length versus feed rate for different beam profiles and laser power settings

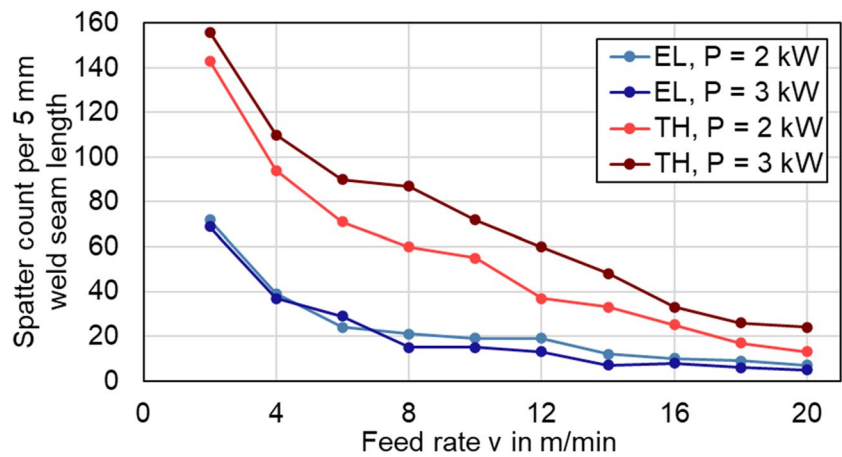


Fig. 20 Maximum intensity projection for laser beam welding of copper using different beam profiles at comparable penetration depth; $\lambda = 515$ nm, EL ($P_L = 2000$ W, $v = 4$ m/min (left)) and TH ($P_L = 1500$ W, $v = 4$ m/min (right))

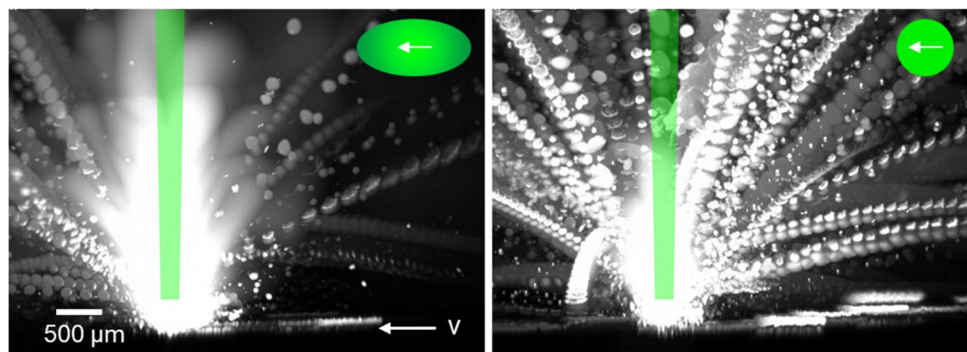
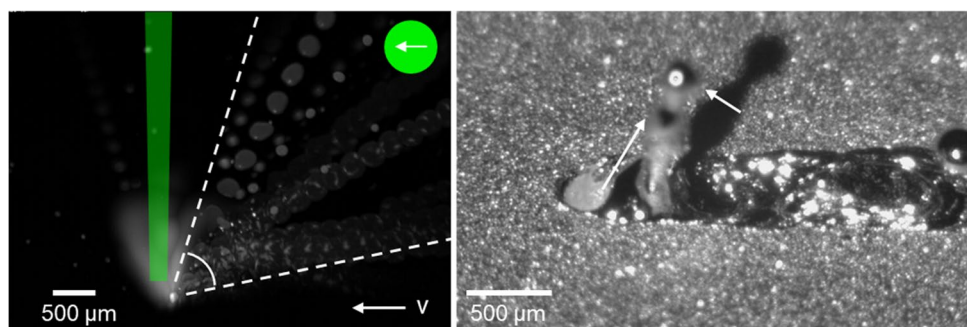


Fig. 21 Maximum intensity projection (left) and example high speed image from the interaction zone (right) for laser beam welding of Cu-ETP using TH beam profile; $\lambda = 515$ nm, $P_L = 2500$ W, and $v = 18$ m/min



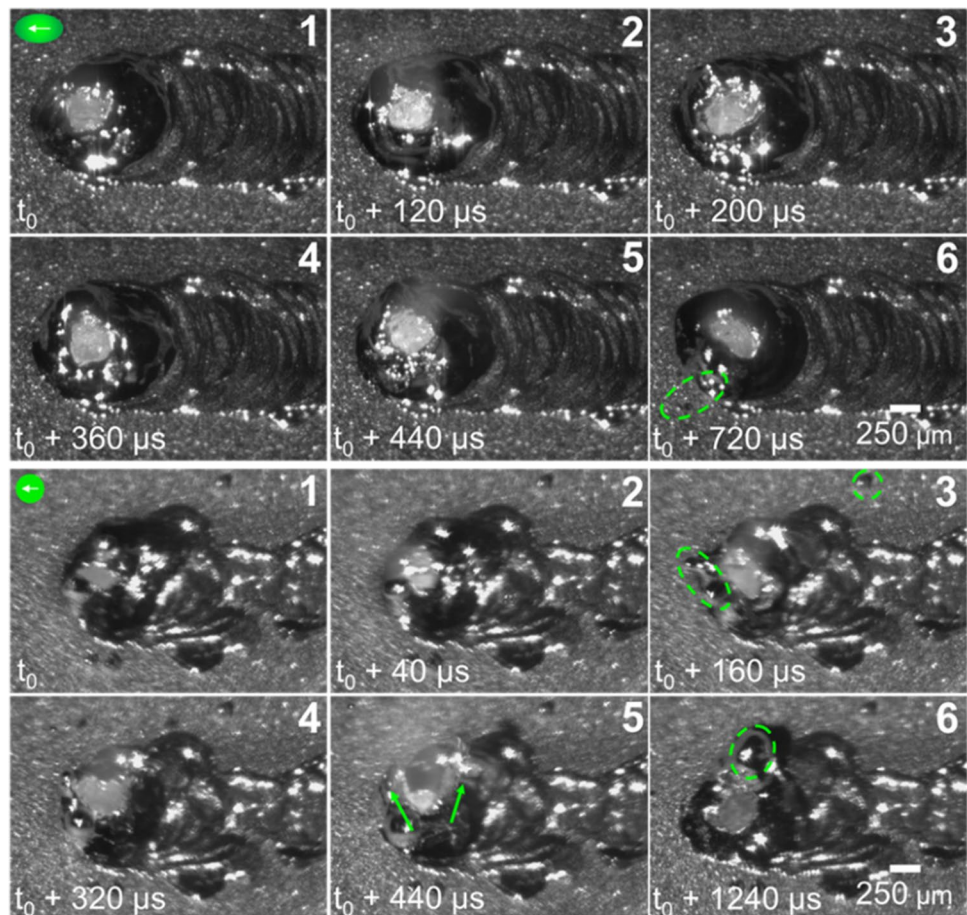
of the corresponding emitted vapor jet, the degree of coupling between the metal vapor plume and the melt pool is influenced, thereby changing its hydrodynamics [57]. The increase of the inclination angle of the former, e.g., by increasing the feed rate and thus increased dynamic pressure of the metal vapor plume, leads to a shift in spatter ejection angle, which coincides with the direction of the plume [58]. However, the reported increase in spatter number with process acceleration on steel is not consistent with the findings of this work investigating copper welding. This behavior is attributed to the lower surface tension of copper, which is 60% of the value of steel at 2000 °C [59].

The reason for the increased process stability in terms of lower spatter count for EL is associated with the steeper edge and the higher energy input in the upper capillary region when using the TH beam profile, exemplary shown in two high speed image sequences in Fig. 22. The lower intensity region in the outer part of the EL beam creates a melt ring around the capillary observed more stable even at short timescale instabilities evident by a pronounced metal vapor plume at $t_0 + 120 \mu\text{s}$, as shown in the upper part of the figure. In the case of $t_0 + 200 \mu\text{s}$, no spatter ejection event was observed subsequent to this instability, with the capillary

opening slightly enlarged again. In images 4–6, a comparable sequence is visible, followed by a spatter ejection event at the front capillary rim (see green dashed line). The slightly increased spatter amount at lower power ($P_L = 2 \text{ kW}$ compared to $P_L = 3 \text{ kW}$) and higher feed rates when using the elliptical beam profile is observed to be caused by the fact that the deep penetration welding process is not fully developed due to the shorter laser-matter interaction time and the wider energy distribution compared to TH (see aspect ratio ~ 1 , Sect. 4.3).

In comparison, strongly fluctuating seam appearance, pronounced spatter formation, and melt ejections with consecutive hole formation are observed for the TH intensity distribution, particularly contributing to the high spatter counts at $v \leq 4 \text{ m/min}$. Figure 22 (bottom) shows seam imperfection formation, where parts of the melt pool are ejected through spatters ($< 100 \mu\text{m}$, frame 3) and larger droplets (frames 5–6). The instabilities are observed starting with liquid copper from the confined melt pool covering parts of the high dynamic capillary opening ($t_0, t_0 + 40 \mu\text{s}$). Due to changed evaporation conditions (increased capillary internal reflections) and associated pressure increase, the upward flow exerts higher frictional forces on the liquid

Fig. 22 Process instabilities in LBW of copper observed through high speed imaging; $\lambda = 515 \text{ nm}$, $P_L = 2000 \text{ W}$, $v = 4 \text{ m/min}$, EL (top) and TH (bottom)



copper interface, tearing material away from the process zone. As discussed above for the low feed rate applied, the ejection direction covers the entire half-space above the specimen (images 3–6).

Since quantification of mass loss during the welding process is easier to investigate compared to imaging techniques, the results are compared below in terms of process stability. The following shares contribute to the measured sample weight reduction: the evaporated material, which is assumed to have a minor impact since no differences could be quantified in the transition mode with the accuracy of the equipment used, wherein evaporation was confirmed by the presence of a metal vapor plume from high-speed image analysis. Moreover, the penetration depth, and thus the capillary depth, is found in comparable dimensions for the beam shapes investigated. So the main share is mass loss from process instabilities in the sense of melt ejection and spatter. Figure 23 (left) presents the average mass loss for varied laser power from $P_L = 2$ kW to $P_L = 3$ kW versus feed rate for both beam profiles. Besides (Fig. 23 right graph), the mass loss ratio, calculated as the ratio of the mass loss to the total molten volume evaluated from the cross-section analysis, is shown.

Comparable trends are visible with regard to the beam profiles and the process parameters. The decrease in mass loss appears to be rather exponential compared to the spatter count and mass loss ratio, where linear trends are observed. The elliptical beam profile reveals the lowest measured values overall, while welds produced with TH are found with significantly increased mass differences prior and after welding, ranging up to 8.5% at $v = 2$ m/min for a laser power of $P_L = 2$ kW. For EL, a mass loss ratio of $\leq 1.2\%$ is measured for all feed rates and laser powers studied. The results in terms of mass loss are thus in good agreement with the observed spatter behavior, and the same resume regarding seam imperfections can be drawn. The presented studies are in excellent agreement with investigations in [34], reporting that the lower energy gradient of the elliptical beam is more

beneficial for improving the stability of the melt pool compared to a Gaussian beam. Results of the simulation of an elliptical capillary shape performed in [42] show that these conditions lead to a reduction in flow velocities in the melt pool and to a lower pressure rise at its tail.

The internal defect amount evaluated by semi-automatic analysis of the cross-sections does not reveal a correlation with the beam profile used. Detailed data analysis shows defect area fractions in the small single-digit value ($< 2\%$, data not shown) of the seam area for all parameter sets, which is assessed to be very low. For slower feed rates up to $v = 6$ m/min, increased pore area ratios were observed, which is assumed to be related to enhanced capillary bulging [60] and altered temperature distribution compared to faster processing speeds. In copper welding investigations focusing on the hairpin welding process, lowest porosity levels in the same order of magnitude are obtained [61] using 515 nm laser radiation.

5 Conclusion

Thanks to the advances in laser development, powerful laser devices with appropriate beam quality are available nowadays, allowing, for example, welding speeds to be increased in laser material processing. With increasing output power of the laser systems, industrial laser welding applications are also becoming more efficient and productive, which can save costs and improve overall profitability. However, for the aforementioned increases, process defects such as pores, spatter, and other process instabilities causing weld seam imperfections must be avoided as best as possible. The aim of this work was therefore the experimental investigation of process characteristics and weld seam imperfection formation in direct comparison of different laser beam shapes using process observation and metallographic analysis for copper welding with green laser radiation. Therefore, a customized welding optics

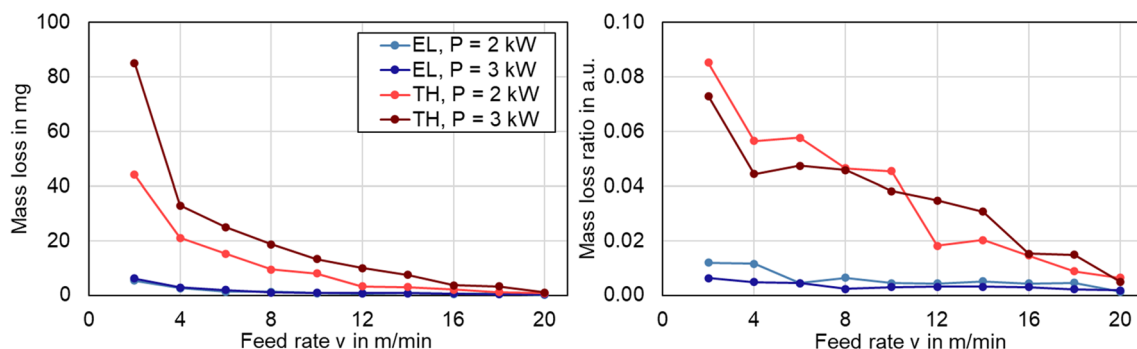


Fig. 23 Absolute mass loss (left) and calculated mass loss ratio (right) versus feed rate for Cu-ETP using different beam profiles and laser power settings

was designed and successfully used in welding trials, producing an elliptical beam shaped by DOE for 515 nm laser radiation with a maximum power of 3 kW. To the knowledge of the authors, this is the first implementation of high-power reflective DOEs for welding application with kW-class beam shaping in copper processing using green laser radiation. To extend the fundamental process understanding, the results were compared with a conventional welding setup using a top hat (flat-top) beam shape. The following conclusions can be drawn:

- An enlarged heat conduction welding regime (7% larger based on feed rate average) is found for the elliptical beam profile in process window analysis, controllable by the orientation of the beam profile in the interaction zone. This regime is almost spatter free and predominantly feasible with visible laser radiation on copper.
- Regarding seam dimensions in deep penetration welding mode, the elliptical beam produces wider joints due to the increased energy input in feed direction compared to a top hat beam profile of same diameter as the minor axis of the ellipse. For the penetration depth, the elliptical beam provides more stable results against feed rate variations.
- For the same processing parameters, a lower melting efficiency (5% on average for all examined parameter sets) is detected for the elliptical beam compared to the top hat, owing to the fact that the aspect ratio of the capillary and thus the capillary internal reflections are increased for the latter.
- The vapor capillary geometries of both beam profiles show comparable parameter dependencies on laser power and feed rate; however, the interaction zone using an elliptical beam profile shows a periodic oscillatory movement in streak image analysis. Measured feature values reveal an increased frequency for increased feed rate and reduced laser power, associated with an inverse behavior of the oscillation amplitude.
- High speed observation of the interaction zone reveals reduced dynamic behavior for the elliptical beam profile compared to the top hat beam profile, correlating with the oscillatory movement of the capillary. Up to 60% less spatters and melt ejections are identified for equal penetration depth. The comparison of the in situ analyses with measured mass loss shows good agreement, emphasizing that the distinct melt pool in the case of the elliptical beam is more tolerant for short time instabilities causing seam imperfection formation.

In sum, the pronounced dynamics in the interaction zone, known for the laser beam welding process of copper, can be effectively reduced using an elliptical shaped laser beam profile. As shown, the change in the energy input leads

to beneficial effects on the formation of seam imperfections using 515 nm laser radiation. Thus, a combination of energy efficiency and precise process guidance in terms of penetration depth and seam imperfection prevention can be achieved. These findings are expected to be beneficial for further process optimization of laser beam welding, especially for applications in the field of electromobility.

As known from practical experience, the transfer of the observed effects in copper to assemblies is challenging, since there is a significant influence of the part geometry on the heat dissipation from the interaction zone, and thus the final weld seam, as well as the effect of scattered radiation in assemblies with neighboring heat-sensitive components, has to be considered. The investigation of these aspects may be the subject of further work.

Acknowledgements We would like to thank C. Wahl and C. Grossert from Midel Photonics GmbH for providing the customized laser beam shaper and the valuable discussion in the collaboration. The support is gratefully acknowledged.

Author Contribution Conceptualization: F.K. Methodology: F.K. Validation: F.K. Formal analysis: F.K. Investigation: F.K. and H.F. Resources: M.S. Data curation: F.K. Writing-original draft preparation: F.K. Writing-review and editing: F.K., S.R. Visualization: F.K. Supervision: S.R. and M.S. Project administration: M.S. Funding acquisition: M.S. All authors have read and agreed to the published version of the manuscript.

Funding Open Access funding enabled and organized by Projekt DEAL. The authors gratefully thank the German Ministry for Economic Affairs and Climate Action for funding part of this work in the research project “GreenPls: Laserbearbeitungseinheit für hochreflektive Werkstoffe” (Grant No KK5004303LP0) as part of the Central Innovation Programme for SMEs.

Data availability The data sets generated during and analyzed during the current study are available from the corresponding author on reasonable request.

Declarations

Ethics approval The authors respect the ethical guidelines of the journal.

Consent to participate Not applicable.

Consent for publication Not applicable.

Conflict of interest The authors declare no competing interests.

Disclaimer The funders had no role in the design of the study; in the collection, analyses, or interpretation of data; in the writing of the manuscript; or in the decision to publish the results.

Open Access This article is licensed under a Creative Commons Attribution 4.0 International License, which permits use, sharing, adaptation, distribution and reproduction in any medium or format, as long as you give appropriate credit to the original author(s) and the source, provide a link to the Creative Commons licence, and indicate if changes were made. The images or other third party material in this article are

included in the article's Creative Commons licence, unless indicated otherwise in a credit line to the material. If material is not included in the article's Creative Commons licence and your intended use is not permitted by statutory regulation or exceeds the permitted use, you will need to obtain permission directly from the copyright holder. To view a copy of this licence, visit <http://creativecommons.org/licenses/by/4.0/>.

References

- Dominioni G (2022) Pricing carbon effectively: a pathway for higher climate change ambition. *Climate Policy* 22:897–905. <https://doi.org/10.1080/14693062.2022.2042177>
- Patel N, Bhoi AK, Padmanaban S et al. (2021) Electric vehicles: modern technologies and trends. *Green energy and technology*. Springer, Singapore
- Pietrzyk S, Tora B (2018) Trends in global copper mining – a review. *IOP Conf Ser Mater Sci Eng* 427:12002. <https://doi.org/10.1088/1757-899X/427/1/012002>
- Das A, Li D, Williams D et al (2018) Joining technologies for automotive battery systems manufacturing. *WEVJ* 9:22. <https://doi.org/10.3390/wevj9020022>
- Hügel H, Graf T (2022) *Materialbearbeitung mit Laser: Grundlagen und Verfahren, 4., überarbeitete und erweiterte Auflage*. Springer eBook Collection. Springer Vieweg, Wiesbaden. <https://doi.org/10.1007/978-3-658-37252-1>
- Kaufmann F, Schrauder J, Hummel M et al (2023) Towards an understanding of the challenges in laser beam welding of copper – observation of the laser-matter interaction zone in laser beam welding of copper and steel using in situ synchrotron x-ray imaging. *Lasers Manuf Mater Process*. <https://doi.org/10.1007/s40516-023-00225-6>
- Volpp J (2017) *Dynamik und Stabilität der Dampfkapillare beim Laserstrahl-tiefschweißen*. Dissertation. Wissen schafft Wirtschaft, Band 63
- Hipp D (2020) *Einkopplung von Laserstrahlung unter Prozessbedingungen der Materialbearbeitung: Entwicklung einer Bestimmungsmethodik und Ergebnisse*. Technische Universität Dresden, Dresden
- Grabmann S, Tomcic L, Zaeh MF (2020) Laser beam welding of copper foil stacks using a green high power disk laser. *Procedia CIRP* 94:582–586. <https://doi.org/10.1016/j.procir.2020.09.080>
- Wang H, Zou Y (2019) Microscale interaction between laser and metal powder in powder-bed additive manufacturing: Conduction mode versus keyhole mode. *Int J Heat Mass Transf* 142:118473. <https://doi.org/10.1016/j.ijheatmasstransfer.2019.118473>
- Hügel H, Graf T (2013) *Laser in der Fertigung: Grundlagen der Strahlquellen, Systeme, Fertigungsverfahren, 3., überarb. und erw. Aufl.* Lehrbuch. Springer Vieweg
- Heider A (2018) *Erweiterung der Prozessgrenzen beim Laserstrahlschweißen von Kupfer mit Einschweiß-tiefen zwischen 1 mm und 10 mm*. Dissertation
- Blom A, Dunias P, van Engen P et al. (2003) Process spread reduction of laser microspot welding of thin copper parts using real-time control. In: *International Society for Optics and Photonics*, pp 493–507. <https://doi.org/10.1117/12.478612>
- Pottlacher G (1999) Thermal conductivity of pulse-heated liquid metals at melting and in the liquid phase. *J Non-Cryst Solids* 250–252:177–181. [https://doi.org/10.1016/S0022-3093\(99\)00116-7](https://doi.org/10.1016/S0022-3093(99)00116-7)
- Nagel F, Kallage P (2020) Increasing the process window of copper welding applications by adapting the power density distribution. *Proceedings of 11th International Conference on Photonic Technologies LANE 2020*
- Helm J, Dietz von Bayer I, Olowinsky A et al (2019) Influence of the surface properties of the connector material on the reliable and reproducible contacting of battery cells with a laser beam welding process. *Weld World* 63:1221–1228. <https://doi.org/10.1007/s40194-019-00727-y>
- Rüttimann C, Dürr U, Moalem A et al. (2011) Reliable laser micro-welding of copper. In: Gu B, Hennig G, Xu X et al. (eds) *Laser Applications in Microelectronic and Optoelectronic Manufacturing (LAMOM) XVI*. SPIE, p 792007. <https://doi.org/10.1117/12.875033>
- Heine L-M, Heider A, Gauch R et al (2023) Blue diode lasers: evaluation of capillary and melt pool dynamics. *J Laser Appl* 35(4). <https://doi.org/10.2351/7.0001092>
- Papastathopoulos E, Bocksrocker O (2022) Advances in beam shaping of high-power CW lasers with BrightLine weld technology. In: Kaielerle S (ed) *High-Power Laser Materials Processing: Applications, Diagnostics, and Systems XI*. SPIE. <https://doi.org/10.1117/12.2607138>
- Punzel E, Hugger F, Dörringer R et al (2020) Comparison of different system technologies for continuous-wave laser beam welding of copper. *Procedia CIRP* 94:587–591. <https://doi.org/10.1016/j.procir.2020.09.081>
- Kaufmann F, Maier A, Ermer J et al. (2021) Influence of defocusing in deep penetration welding of copper by using visible wavelength. *Proceedings of the 11th International WLT-Conference on Lasers in Manufacturing*. WLT - Wissenschaftliche Gesellschaft Lasertechnik e.V., Munich
- Alter L, Heider A, Bergmann J-P (2018) Investigations on copper welding using a frequency-doubled disk laser and high welding speeds. *Procedia CIRP* 74:12–16
- Katayama S (ed) (2013) *Handbook of laser welding technologies : woodhead publishing series in electronic and optical materials*. Woodhead Publishing
- Alter L, Heider A, Bergmann JP (2020) Influence of hydrogen, oxygen, nitrogen, and water vapor on the formation of pores at welding of copper using laser light at 515 nm wavelength. *J Laser Appl* 35(3). <https://doi.org/10.2351/7.0000063>
- EN ISO 6520 *Welding and allied processes - classification of geometric imperfections in metallic materials - Part 1: Fusion welding*. Beuth Verlag, Berlin
- Franco D (2017) *Wobbling laser beam welding of copper*. Dissertation, Universidade Nova De Lisboa
- Heider A, Weber R, Herrmann D et al (2015) Power modulation to stabilize laser welding of copper. *J Laser Appl* 27:22003. <https://doi.org/10.2351/1.4906127>
- Kaufmann F, Forster C, Hummel M et al (2023) Characterization of vapor capillary geometry in laser beam welding of copper with 515 nm and 1030 nm laser beam sources by means of in situ synchrotron x-ray imaging. *Metals* 13:135. <https://doi.org/10.3390/met13010135>
- Kaplan AFH, Powell J (2011) Spatter in laser welding. *J Laser Appl* 23:32005. <https://doi.org/10.2351/1.3597830>
- Zhang G, Zhu B, Zou J et al (2020) Correlation between the spatters and evaporation vapor on the front keyhole wall during fiber laser keyhole welding. *J Market Res* 9:15143–15152. <https://doi.org/10.1016/j.jmrt.2020.10.103>
- Katayama S, Kawahito Y, Mizutani M (2012) Latest progress in performance and understanding of laser welding. *Phys Procedia* 39:8–16. <https://doi.org/10.1016/j.phpro.2012.10.008>
- Schneider A, Avilov V, Gumenyuk A et al (2013) Laser beam welding of aluminum alloys under the influence of an electromagnetic field. *Phys Procedia* 41:4–11. <https://doi.org/10.1016/j.phpro.2013.03.045>
- Fabbro R (2010) Melt pool and keyhole behaviour analysis for deep penetration laser welding. *J Phys D: Appl Phys* 43:445501. <https://doi.org/10.1088/0022-3727/43/44/445501>

34. Bi J, Wu L, Li S et al (2023) Beam shaping technology and its application in metal laser additive manufacturing: a review. *J Market Res* 26:4606–4628. <https://doi.org/10.1016/j.jmrt.2023.08.037>
35. Katz S, Kaplan N, Grossinger I (2018) Using diffractive optical elements. *Optik & Photonik* 13:83–86. <https://doi.org/10.1002/opph.201870416>
36. Liu X, Cheng CH (2004) System and method of laser drilling (U.S. Patent No. 6,720,519)
37. Hansen KS, Kristiansen M, Olsen FO (2014) Beam shaping to control of weldpool size in width and depth. *Phys Procedia* 56:467–476. <https://doi.org/10.1016/j.phpro.2014.08.150>
38. Kang S, Shin J (2021) Laser beam oscillation welding of aluminum alloy using the spatially modulated beam by diffractive optical element (DOE). *J Manuf Process* 66:387–396. <https://doi.org/10.1016/j.jmapro.2021.04.029>
39. Sundqvist J, Kaplan A, Shachaf L et al (2017) Analytical heat conduction modelling for shaped laser beams. *J Mater Process Technol* 247:48–54. <https://doi.org/10.1016/j.jmatprotec.2017.04.011>
40. Volpp J, Vollertsen F (2013) Analytical modeling of the keyhole including multiple reflections for analysis of the influence of different laser intensity distributions on keyhole geometry. *Phys Procedia* 41:460–468. <https://doi.org/10.1016/j.phpro.2013.03.102>
41. Matthews MJ, Roehling TT, Khairallah SA et al (2020) Controlling melt pool shape, microstructure and residual stress in additively manufactured metals using modified laser beam profiles. *Procedia CIRP* 94:200–204. <https://doi.org/10.1016/j.procir.2020.09.038>
42. Beck M (1996) Modellierung des Lasertiefschweißens. Doctoral Thesis, Universität Stuttgart, Teubner Verlag, Leipzig
43. Glumann C (1996) Verbesserte Prozesssicherheit und Qualität durch Strahlkombination beim Laserschweißen. Stuttgart, Univ., Diss. Laser in der Materialbearbeitung. Teubner, Stuttgart, Zugl.
44. Abe N, Funada Y (2008) Micro welding of thin foils with an elliptical beam of direct diode laser. In: Zhong M (ed) Conference proceedings 2008: Plenary session. Laser Institute of America, Orlando, FL, pp 930–935. <https://doi.org/10.2351/1.5057156>
45. Noori Rahim Abadi S, Mi Y, Sikström F et al (2021) Effect of shaped laser beam profiles on melt flow dynamics in conduction mode welding. *Int J Therm Sci* 166:106957. <https://doi.org/10.1016/j.ijthermalsci.2021.106957>
46. Nahr F, Bartels D, Rothfelder R et al (2023) Influence of novel beam shapes on laser-based processing of high-strength aluminum alloys on the basis of EN AW-5083 single weld tracks. *JMMP* 7:93. <https://doi.org/10.3390/jmmp7030093>
47. Kaufmann F, Maier A, Schrauder J et al (2022) Influence of superimposed intensity distributions on weld seam quality and spatter behavior during laser beam welding of copper with green laser radiation. *J Laser Appl* 34:42008. <https://doi.org/10.2351/7.0000771>
48. Sundqvist J, Kaplan A, Shachaf L et al (2016) Numerical optimization approaches of single-pulse conduction laser welding by beam shape tailoring. *Opt Lasers Eng* 79:48–54. <https://doi.org/10.1016/j.optlaseng.2015.12.001>
49. Kaufmann F, Ermer J, Maier A et al. (2021) Influence of plume attenuation under high power laser welding of copper using visible wavelengths. *J Laser Appl* 33(4). <https://doi.org/10.2351/7.0000505>
50. Kaufmann F, Maier A, Schrauder J et al. (2023) Influence of laser beam intensity distribution on keyhole geometry and process stability using green laser radiation. In: Silva FJG, Pereira AB, Campilho RDSG (eds) Flexible automation and intelligent manufacturing: establishing. Springer International, PU, pp 216–227. https://doi.org/10.1007/978-3-031-38241-3_25
51. Graf T, Berger P, Weber R et al (2015) Analytical expressions for the threshold of deep-penetration laser welding. *Laser Phys Lett* 12:56002
52. Tang Z, Wan Le, Yang H et al (2024) Stable conduction mode welding of conventional high-reflectivity metals with 2000 W blue laser. *Opt Laser Technol* 168:109971. <https://doi.org/10.1016/j.optlastec.2023.109971>
53. Helm J (2022) Prozessstabilität und Prozesseffizienz beim Laserstrahlfügen von hoch reflektiven Kupferwerkstoffen, 1st edn. Apprimus Verlag, Aachen, Ergebnisse aus der Lasertechnik
54. Takenaka K, Sato Y, Fujio S et al (2023) Bead-on-plate welding of pure copper with a 1.5-kW high-power blue diode laser. *Weld World* 67:99–107. <https://doi.org/10.1007/s40194-022-01401-6>
55. Poprawe R (2011) Tailored light 2: laser application technology. RWTHeDition. Springer Berlin Heidelberg, Berlin, Heidelberg. <https://doi.org/10.1007/978-3-642-01237-2>
56. Fetzer F, Hagenlocher C, Weber R et al (2021) Geometry and stability of the capillary during deep-penetration laser welding of AlMgSi at high feed rates. *Opt Laser Technol* 133:106562. <https://doi.org/10.1016/j.optlastec.2020.106562>
57. Weberpals J, Dausinger F (2007) Influence of inclination angle on spatter behavior at welding with lasers of strong focusability. In: Congress proceedings 2007. Laser Institute of America, Orlando, Fla, p 1602. <https://doi.org/10.2351/1.5061015>
58. Fabbro R, Slimani S, Coste F et al. (2007) Analysis of the various melt pool hydrodynamic regimes observed during cw Nd-YAG deep penetration laser welding. In: Congress proceedings 2007. Laser Institute of America, Orlando, Fla, p 802. <https://doi.org/10.2351/1.5061093>
59. Yaws CL (2015) The Yaws handbook of physical properties for hydrocarbons and chemicals: Physical properties for more than 54,000 organic and inorganic chemical compounds, coverage for C1 to C100 organics and ac to zr inorganics, Second edition. Elsevier Science GPP, Amsterdam [u.a.]
60. Fetzer F, Hu H, Berger P et al. Pores in laser beam welding: generation mechanism and impact on the melt flow. In: Kaierle, Heinemann (Hg.) – High-power laser materials processing, p 12. <https://doi.org/10.1117/12.2295798>
61. D’Arcangelo S, Caprio L, Chesi D et al (2024) Comprehensive benchmarking of laser welding technologies including novel beam shapes and wavelengths for e-drive copper hairpins. *Opt Laser Technol* 169:109964. <https://doi.org/10.1016/j.optlastec.2023.109964>

Publisher's Note Springer Nature remains neutral with regard to jurisdictional claims in published maps and institutional affiliations.